

Article

Study on the Effect of Supplementary Cementitious Material on the Regeneration Performance of Waste Fresh Concrete

Weicheng Wang ¹, Daoming Zhang ^{2,*}, Linqing Liu ³, Xueyuan Zhang ² and Yue Wang ¹¹ College of Materials Science and Engineering, Qiqihar University, Qiqihar 161006, China² College of Architecture and Civil Engineering, Qiqihar University, Qiqihar 161006, China³ Chengbang Ecological Environment Co., Ltd., Hangzhou 310008, China

* Correspondence: zdmzdm@sina.com

Abstract: In the preparation of ready-mixed concrete, it is inevitable to produce waste fresh concrete (WFC). An efficient, low-cost and environmentally friendly recycling scheme is the key to WFC recycling. In this work, we directly added some unhardened WFC to fresh concrete to prepare recycled fresh concrete (RFC); on this basis, fly ash (FA) and nano-silica (NS) were added as supplementary cementitious material (SCM) to obtain modified recycled fresh concrete (RFC-SF). Then, the mechanical properties, slump, freeze–thaw resistance, phase structure of the hydration products and hydration process in RFC were studied. The results show that the addition of FA and NS significantly improved the comprehensive performance of RFC. Compared with RFC, the compressive strength of RFC-SF with 15% FA and 3% NS increased by 15.2% and 50.3% at 7 d and 90 d, respectively, and the splitting tensile strength increased by 20.5% and 76.4%, respectively. The slump remained above 155 mm, and the mass loss rate decreased by 42.6% after freeze–thaw cycles. XRD and FTIR analysis showed that the addition of FA and NS accelerated the hydration reaction process of RFC-SF, reduced the content of calcium hydroxide (CH) and refined the grain size of CH. RFC-SF had a denser microstructure and a lower calcium-silicon ratio in SEM and EDS tests.

Keywords: waste fresh concrete; recycled fresh concrete; supplementary cementitious material; mechanical properties; fly ash; nano-silica; microcharacterization



Citation: Wang, W.; Zhang, D.; Liu, L.; Zhang, X.; Wang, Y. Study on the Effect of Supplementary Cementitious Material on the Regeneration Performance of Waste Fresh Concrete. *Buildings* **2023**, *13*, 687. <https://doi.org/10.3390/buildings13030687>

Academic Editor: Zengfeng Zhao

Received: 27 November 2022

Revised: 14 December 2022

Accepted: 20 December 2022

Published: 6 March 2023



Copyright: © 2023 by the authors. Licensee MDPI, Basel, Switzerland. This article is an open access article distributed under the terms and conditions of the Creative Commons Attribution (CC BY) license (<https://creativecommons.org/licenses/by/4.0/>).

1. Introduction

As the main material in infrastructure construction, annual global concrete production has exceeded 27 billion tons [1,2], of which 3% of the daily output is abandoned due to improper mix ratio and over time during transportation and pouring [3,4]. Recycling and reusing waste construction materials can improve the recycling rate of building materials, reduce the space required to bury waste and reduce pollution to the air environment [5–9]. For the waste fresh concrete (WFC) produced during the production of ready-mixed concrete, the traditional regeneration method often uses aggregate washing and screening to separate the aggregate and mud to prepare recycled concrete [10–13], while the wastewater and residue produced during washing can be put into concrete production again [14,15]. The waste slurry in WFC can be used as a curing agent to fill in the soil and road base to improve the stability of the soil structure [16,17]. Since the waste slurry is alkaline and rich in calcium, it can also be used as a chemical adsorbent in CO₂ capture, phosphorus recovery and water purification [18–20].

Compared with the traditional regeneration method, the more novel and rapid way is to use WFC as a part of ready-mixed concrete, directly stirred in to prepare recycled fresh concrete (RFC), and modify the RFC to reapply it in the field of engineering construction [21]. This regeneration method has the characteristics of lower energy consumption, a simpler site environment and a shorter regeneration production cycle. Some researchers have added retarders and accelerators to the WFC to adjust the setting time of the WFC, and

then mixed it with ready-mixed concrete to be used in construction projects again [22–25]. Xuan et al. put the unhardened WFC paste directly into cement and recycled aggregate to prepare concrete blocks, and then carbonized the prepared blocks to enhance the mechanical properties of the blocks [21].

The above WFC regeneration methods have improved the recycling rate of building materials. However, more efficient, convenient and low-cost modification methods must be explored. Adding supplementary cementitious material (SCM) for modification when preparing RFC directly from unhardened WFC may be a more convenient and inexpensive recovery method. With the rapid development of building materials, SCM has become an important measure to improve the regeneration performance of concrete [26]. Among them, the addition of CNT, GNPs and nano-silica (NS) as SCMs can significantly improve the mechanical properties of concrete [27–29]. Compared with CNT and GNPs, NS is low cost and simple to use; moreover, NS has the advantages of high permeability, high specific surface energy, nucleation and pozzolanic effect. Its incorporation into cement-based materials can effectively enhance hydration activity, accelerate the hydration rate and improve the mechanical properties of concrete [30,31]. However, a large number of unsaturated bonds in NS can easily absorb free water, which seriously affects the working performance of concrete [32]. The fly ash (FA) in SCM can significantly improve the working performance and durability of concrete due to its small size and the morphological characteristics of glass spheres [33,34]. On the other hand, the chemical activity of FA is lower than that of cement, and excessive incorporation is not conducive to the improvement of the early strength of concrete [35].

It can be seen that when these two materials are separately mixed with WFC for direct regeneration, the prepared RFC has problems such as low early strength and poor working performance. If these two materials are mixed together, however, then these problems may be mitigated [36]. In this study, FA and NS were mixed into RFC, and the effects of different proportions of FA and NS on the strength, slump and freeze–thaw resistance of RFC were analyzed as well as the changes of phase composition and microstructure after adding these two materials. The results of this study provide a valuable method for the direct recycling of WFC.

2. Materials and Methods

2.1. Materials

P.O42.5 ordinary Portland cement produced by Qiqihar Beijiang company (Qiqihar City and China) was used, and grade I ash was used for fly ash. Table 1 shows the chemical composition of the cement and fly ash used under XRF analysis, in which it can be seen that the fly ash was a low-calcium type. The sand was medium sand produced locally in Qiqihar, and the fineness modulus was 2.3. Gravel with a continuous gradation range of 5–25 mm was used. The model of water-reducing agent is 325C polycarboxylic superplasticizer (PS). The NS was a transparent liquid from Suzhou Nadi Microelectronics Co., LTD (Suzhou City and China). Table 2 gives the properties of the NS liquid.

Table 1. Chemical compositions of cement and fly ash (%).

Materials	SiO ₂	Al ₂ O ₃	CaO	Fe ₂ O ₃	MgO	K ₂ O	Na ₂ O	Cr ₂ O ₃	Others
cement	31.5	10.7	46.19	3.93	3.31	1.31	0.76	/	2.3
fly ash	40.1	29.3	3.69	14.9	0.81	1.13	0.58	5.94	3.55

Table 2. Performance parameters of NS (%).

Exterior	Average Particle Size/nm	Content/%	Solvent	pH Value
Transparent liquid	15 ± 5	30	Transparent liquid	9–11

The setting time of fresh concrete is an important factor affecting the working performance of concrete and the hydration performance of slurry [37]. Consequently, normal concrete (NC) with a water–binder ratio of 0.5 and cement paste with the same ratio (NC-J) were prepared, and each cubic meter contains 180 kg of water, 360 kg of cement, 760 kg of sand, 1100 kg of gravel and 2.52 kg of PS. Then, the slump of NC at 120 min, 180 min and 300 min was tested, and the performance changes of NC-J in these three time periods were analyzed with a Fourier transform infrared spectrometer. Figure 1 shows that the slump of NC presents a plummeting trend with the increase of setting time, and its morphology changes from plastic slurry to angular block with aggregate wrapped by slurry, which cannot be poured. Figure 2 shows that the absorption peak of C_3S dominated by Si-O bond vibration is mainly reflected at 930 cm^{-1} after mixing NC-J for 120 min. When the standing time was extended to 180 min and 300 min, the vibration absorption peak of Si-O bond did not migrate from the low wavenumber to a high wavenumber. This indicates that the slurry was still in the hydration induction period during this period [38], and C_3S did not enter the rapid hydration reaction period and still has strong reactivity. Considering that the initial setting time of cement used is 180 min, we collected concrete that lost its plasticity after being placed for 180 min as WFC.

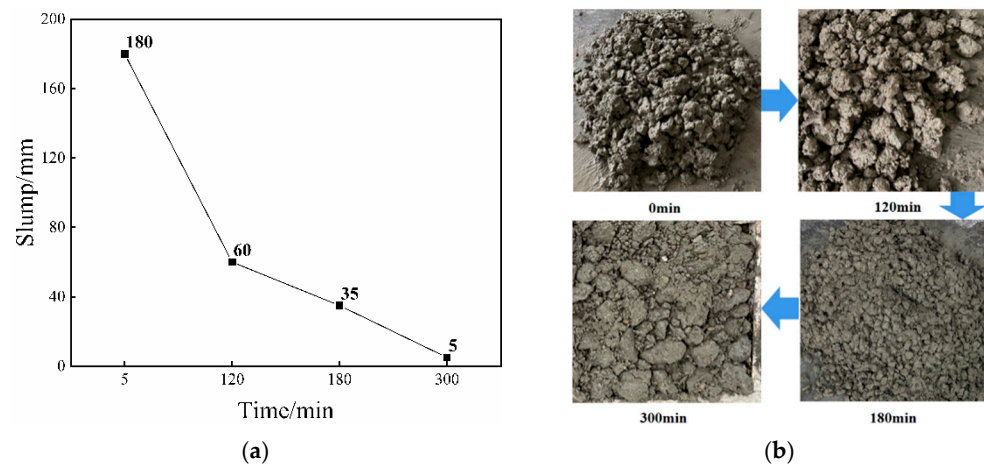


Figure 1. Working performance of concrete under different placement times. (a) Slump of concrete; (b) Morphology of concrete.

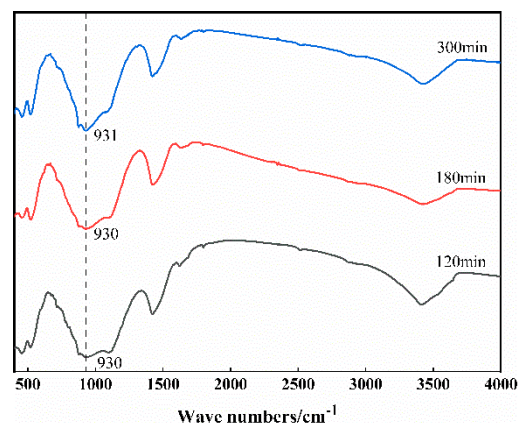


Figure 2. FTIR spectrum of NC-J at early hydration.

2.2. Methods

2.2.1. Proportioning of Concrete

In order to explore the effects of different FA and NS additions on RFC performance in this study, 14 groups of concrete mixing ratios were designed, and the water–binder ratio of each group was 0.5. Among these groups, NC was normal concrete; RFC was the

concrete directly prepared with WFC replacing NC at a replacement rate of 30% of the total mass of NC; RFC-F was RFC with FA added separately as SCM; RFC-SF was the composite addition of FA and NS to the RFC. NC, RFC, RFC-F and RFC-SF all had variations designed with cement paste with the same ratio as concrete for microscopic performance testing, and they were recorded as NC-J, RFC-J, RFC-F-J and RFC-SF-J. For example, RFC-S3F15 represents the addition of 15% FA and 3% NS to RFC, and RFC-S5F20-J represents the addition of 20% FA and 5% NS to RFC-J. In order to effectively control the influence of the water–binder ratio, the additional water contained in NS was subtracted from the mixing water of RFC-SF. In addition, when preparing for mixing water, NS and PS were put into water to mix together and then dispersed with ultrasonic waves, which can eliminate the agglomeration phenomenon of nanomaterials due to the high specific surface energy [39]. Table 3 shows the mix ratios of concrete and cement pastes.

Table 3. Mixture proportions of concrete and the same proportion of cement pastes (kg/m³).

Samples	Cement	Water	Cement Paste			Additional Water	Aggregate		WFC
			FA	NS	PS		Sand	Gravel	
NC	360	180	-	-	2.5	-	760	1100	-
RFC	252	126	-	-	1.8	-	532	770	720.7
RFC-F10	216	126	36	-	1.8	-	532	770	720.7
RFC-F15	198	126	54	-	1.8	-	532	770	720.7
RFC-F20	180	126	72	-	1.8	-	532	770	720.7
RFC-S1F10	214.9	123.5	36	3.6	1.8	2.5	532	770	720.7
RFC-S3F10	212.8	118.4	36	10.8	1.8	7.6	532	770	720.7
RFC-S5F10	210.6	113.4	36	18	1.8	12.6	532	770	720.7
RFC-S1F15	196.9	123.5	54	3.6	1.8	2.5	532	770	720.7
RFC-S3F15	194.8	118.4	54	10.8	1.8	7.6	532	770	720.7
RFC-S5F15	192.6	113.4	54	18	1.8	12.6	532	770	720.7
RFC-S1F20	178.9	123.5	72	3.6	1.8	2.5	532	770	720.7
RFC-S3F20	176.8	118.4	72	10.8	1.8	7.6	532	770	720.7
RFC-S5F20	174.6	113.4	72	18	1.8	12.6	532	770	720.7

2.2.2. Slump and Mechanical Properties

The concrete steps of the slump test conform to the Chinese standard GB/T 50080-2002. After the slump test, the concrete samples were put into concrete molds and then demolded after 24 h. In order to better meet the requirements of the specimen size in the frost resistance test, the concrete test blocks in this test were designed with a size of 100 mm × 100 mm × 100 mm. Then, the samples were placed in a curing room (T = 20 ± 2 °C, RH > 95%) for 7 days, 28 days and 90 days. After reaching the curing age, according to the Chinese standard GB/T 50081-2019, the compressive strength and splitting tensile strength of concrete samples were tested with the YAW-2000 pressure testing machine.

2.2.3. Freeze–Thaw Resistance

The freeze–thawing test of concrete adopted the slow-freezing method in Chinese standard GB/T 50082-2009. Firstly, as shown in Figure 3a, the concrete samples that had been cured for 24 days were immersed in water (T = 20 ± 2 °C) for 4 days. After the immersion was completed, the surface water of the samples was wiped off, and then the samples were weighed. Then, as shown in Figure 3a, the samples were put into the freeze–thaw testing machine for 150 freeze–thaw cycles, each freeze–thaw cycle taking 8 h. The temperature in the freeze–thaw machine was (−20~−18 °C) when frozen, and the water temperature was (18~20 °C) when melted. After 25 cycles, the test blocks were weighed. Finally, the mass loss rate of the concrete samples was calculated and averaged.



Figure 3. Freeze–thaw testing. (a) Specimen immersion; (b) specimen freeze–thaw.

2.2.4. Microstructure Analysis

Various micro-experiments were conducted to evaluate the microstructure and components of concrete and its cement pastes, which helped to analyze the macro properties and regeneration mechanisms of each group of RFC samples. Phase analysis of the paste was performed at a scanning rate of $4^\circ/\text{min}$ using an X-ray diffractometer (XRD, Smart Lab 9Kw, Rigaku, Tokyo, Japan) with $\text{CuK}\alpha$ radiation. The hydration process of RFC was analyzed with the Fourier transform infrared spectrometer (FTIR, Nicolet 6700, Thermo Scientific, Waltham, MA, USA) in the range of $400\text{--}4000\text{ cm}^{-1}$. The microstructure of RFC was analyzed with a scanning electron microscope (SEM, S-4300, Hitachi, Tokyo, Japan) and an energy-dispersive X-ray spectrometer (EDS, Quantax75, Hitachi, Tokyo, Japan).

3. Results

3.1. Mechanical Properties

3.1.1. Effect of Adding Fly Ash Alone

It can be observed from Figure 4 that the strength of RFC at any curing age is lower than that of NC, and that the addition of FA alone has a negative effect on the early mechanical properties of RFC. Figure 4a shows that the compressive strength of RFC-F with FA is significantly lower than that of RFC at 7 d and 28 d, and this situation becomes more obvious with the addition of FA. When the curing age was extended to 90 d, the compressive strength of RFC-F exceeded that of RFC, and the compressive strength of RFC-F10, RFC-F15 and RFC-F20 increased by 22.8%, 25.6% and 17.3%, respectively. In addition, the increasing rate of compressive strength of RFC-F is greater than that of NC in 28–90 d.

A similar situation also occurs in splitting tensile strength. Figure 4b shows that the splitting tensile strength of RFC is lower than that of NC at any curing age; the splitting tensile strength of RFC-F at 7 d and 28 d is also lower than that of RFC. When the curing age increased to 90 d, the splitting tensile strength of RFC-F10, RFC-F15 and RFC-F20 increased by 39.7%, 44.2% and 32.2%, respectively, compared with RFC.

The reason for the above phenomenon is that the polymerization degree of $[\text{SiO}_4]^{4-}$ in FA is large, and most instances were long chain polymerization, which is not easy to disintegrate and fracture. Moreover, the surfaces of glass beads in FA were dense and smooth, and the erosion process of OH^- is slow, which delayed the reaction of Ca^{2+} and OH^- to form C-S-H, thus affecting the improvement of early strength. When age was increased, OH^- was eroded into the glass beads and a pozzolanic reaction occurred; this reaction increased the content of C-S-H and improved the strength of RFC-F.

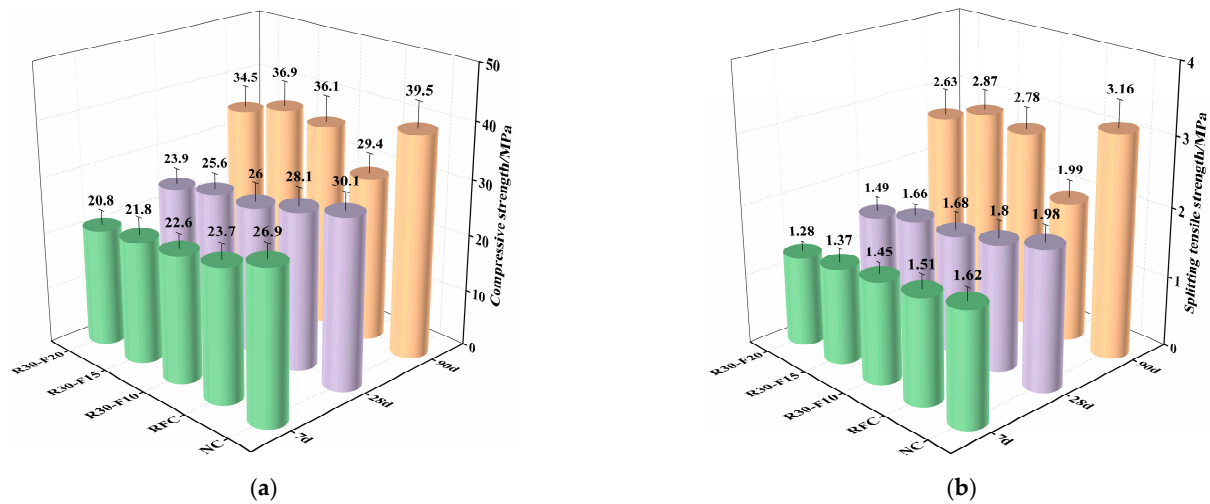


Figure 4. Mechanical properties of RFC-F with FA. (a) Compressive strength; (b) splitting tensile strength.

3.1.2. Effect of Composite Addition of Fly Ash and Nano-Silica

On the basis of adding FA, FA and NS were mixed into RFC, and the effect of the two materials on RFC was tested. Figure 5a clearly shows the compressive strength change trend of RFC-SF with FA and NS. When the curing age was 7 d, the compressive strength of RFC-S3F15 was 15.2% higher than that of RFC. This indicates that the addition of NS effectively compensates for the deterioration of early compressive strength of RFC caused by fly ash. When the curing age was extended to 90 d, the compressive strength of RFC-SF increased by 9.5~50.3% compared with RFC. Figure 5b shows the splitting tensile strength of RFC-SF with two materials at 7 d, 28 d and 90 d. Similar to compressive strength, the splitting tensile strength of RFC-S3F15 at 7 d was 20.5% higher than that of RFC. The splitting tensile strength of RFC-SF increased by 10.1~76.4% at 90 d, and some results were higher than that of NC.

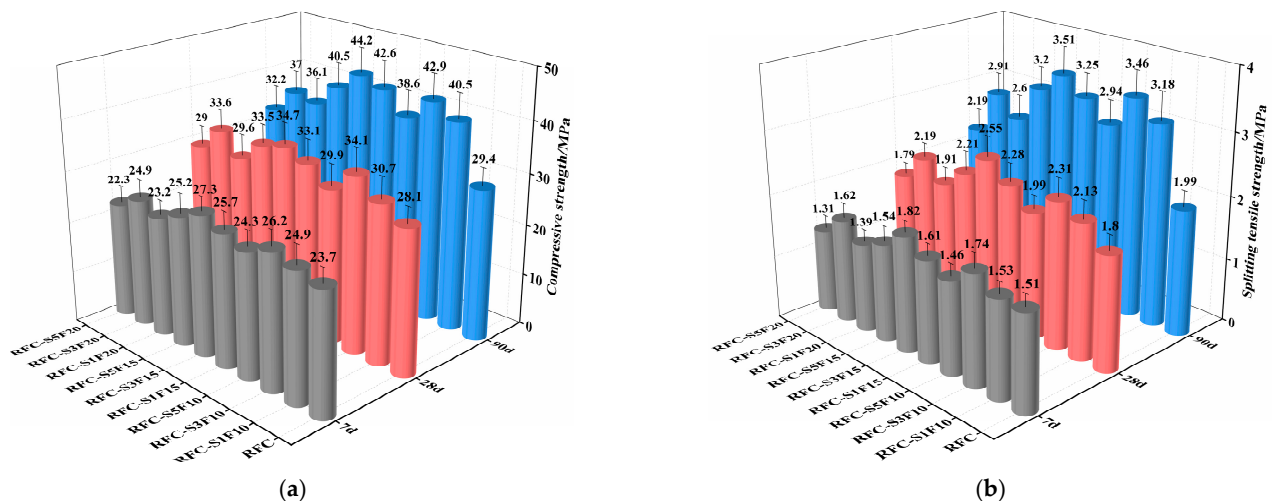


Figure 5. Mechanical properties of RFC-SF with FA and NS. (a) Compressive strength; (b) splitting tensile strength.

The above strength improvement is due to the synergistic effect between FA and NS [40]. In the early stage of the reaction, the fine particles of FA are evenly distributed, which prevents the mutual cohesion between cement particles and provides them with a larger surface area for hydration reaction. The addition of highly active NS can significantly

accelerate the hydration reaction rate of cement and improve the early strength of concrete. In addition, calcium hydroxide (CH) in cement hydration products can also undergo secondary hydration reactions with SiO_2 and increase the content of C-S-H in cement stone. In the later stages, the volcanic ash activity of FA is reflected. These measures provide RFC-SF with stronger mechanical properties.

It should be noted that with the increase of the amount of the two materials, the strength of RFC-SF first increases and then decreases. This is because too much nano SiO_2 agglomerates together, which absorbs free water and delays the hydration reaction of cement. Similarly, excessive introduction of low-activity FA will reduce hydration reactivity, which adversely affects the strength of RFC-SF.

3.2. Slump

The slump of concrete containing different contents of FA and NS is shown in Figure 6. After mixing for 5 min, the slumps of NC and RFC remained at about 180 mm and 150 mm, respectively. In contrast, the addition of FA increased the slump of RFC-F to above 185 mm, gradually increasing with the increase of FA content. When FA and NS were added together, the slump of RFC-SF was between 120 and 185 mm, and some of them were still larger than RFC. The reason for the decrease in slump is that NS has a very high specific surface energy, which makes a large number of unsaturated bonds absorb free water and form uneven hydration flocs [41], thereby reducing the free water content in RFC-SF. However, FA with smooth surfaces and fine particle size can disperse this part of the hydration flocs so that more water molecules absorbed by the flocs are freed, and its small spherical morphology makes it play a lubricating role in mixing, reducing the friction resistance between concrete aggregates.

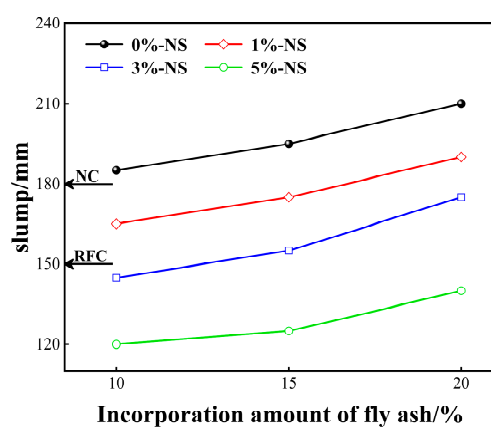


Figure 6. Slump of concrete with different contents of FA and NS.

3.3. Freeze–Thaw Resistance

Figure 7a shows the trend of mass loss rate of NC, RFC and RFC-F under 150 freeze–thaw cycles. In the early stage of freeze–thaw cycles, the mass loss rate of NC, RFC and RFC-F were negative. With the increase of freeze–thaw cycles, the mass loss rates gradually became positive and showed upward trends. After 150 freeze–thaw cycles, the mass loss rate of RFC-F with FA was between 0.32 and 0.43% as compared with RFC, and the mass loss rate of RFC-F15 decreased by 31.9%. In the early stage of the freeze–thaw cycle, high porosity concrete absorbed a lot of water when immersed in water, which increased the quality of concrete and led to a negative mass loss rate. After long-term freeze–thaw action, the water in the pores produced expansion stress and increased continuously when frozen, which caused the destruction of the concrete pore structure, made the cement paste and fine aggregate at the corner of the samples appear to be obviously spalling, and reduced the quality of concrete. This phenomenon is most obvious in unmodified RFC. However, FA with small particle size and microsphere morphology has filled the pores in RFC-F, which reduced the porosity of RFC and weakened the adverse effect of the expansion stress of

freezing water on the pore structure, which makes RFC-F have a smaller mass loss rate and good freeze–thaw resistance.

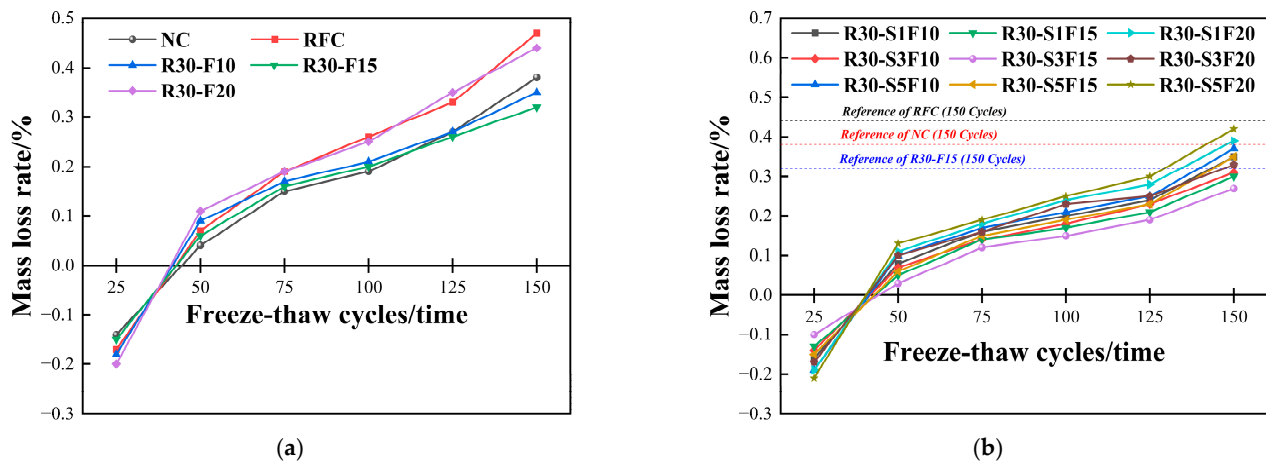


Figure 7. Mass loss rates of RFC-F and RFC-SF after freeze–thaw cycles. (a) RFC-F; (b) RFC-SF.

Figure 7b shows that the composite addition of FA and NS can improve the freeze–thaw cycle performance of RFC-SF more obviously. The freeze–thaw cycle loss rate of RFC-SF was between 0.27 and 0.42%. Compared with RFC, the mass loss rate of RFC-S3F15 decreased by 42.6%. This is due to the addition of NS to generate more C–S–H on the basis of FA, which enhanced the strength of cement stone. At the same time, the nano-sized SiO₂ also filled some capillary pores, reduced the porosity and optimized the pore structure, which mitigated the damage caused by the expansion stress of freezing water to the pore structure and further improved the freeze–thaw resistance of RFC-SF.

3.4. Microstructure Analysis

3.4.1. XRD

The phase composition of different cement paste samples cured for 7 d and 28 d were measured with XRD, as shown in Figure 8a. It can be seen that the mineral types of RFC-F-J with FA added and RFC-SF-J with FA and NS added are basically the same as those of NC-J. However, the intensity of C₂S and C₃S in RFC-F15-J with FA is higher than that in NC-J and RFC-J, and the intensity of CH is lower than that in NC-J and RFC-J. This indicates that in the early stage of hydration reaction, the addition of FA with low activity delays the hydration reaction, resulting in a higher content of C₃S and C₂S in the unreacted cement clinker in the cement paste and lower C–S–H and CH content in the hydration products, which is an important factor in the poor early strength of RFC-F. In contrast, the intensities of the C₂S, C₃S and CH of RFC-S3F15-J with two materials are lower than that of RFC-J and RFC-F-J, which is because the addition of NS promotes the hydration reaction. In addition, CH also reacts with SiO₂ to further consume it, which increases the C–S–H content. The XRD spectrum of Figure 8b shows that the intensities of the C₃S, C₂S and CH of RFC-S3F15 are still lower than that of RFC after 28 days of cement paste curing, which indicates that the addition of the two materials is still helpful for the hydration reaction at a longer age. Moreover, the CH intensity of RFC-F15-J is lower than that of RFC, which may be due to the fact that the Si–O and Al–O bonds in FA are eroded by OH[−] and Ca²⁺ with strong polarity, and CH is consumed by reaction with them.

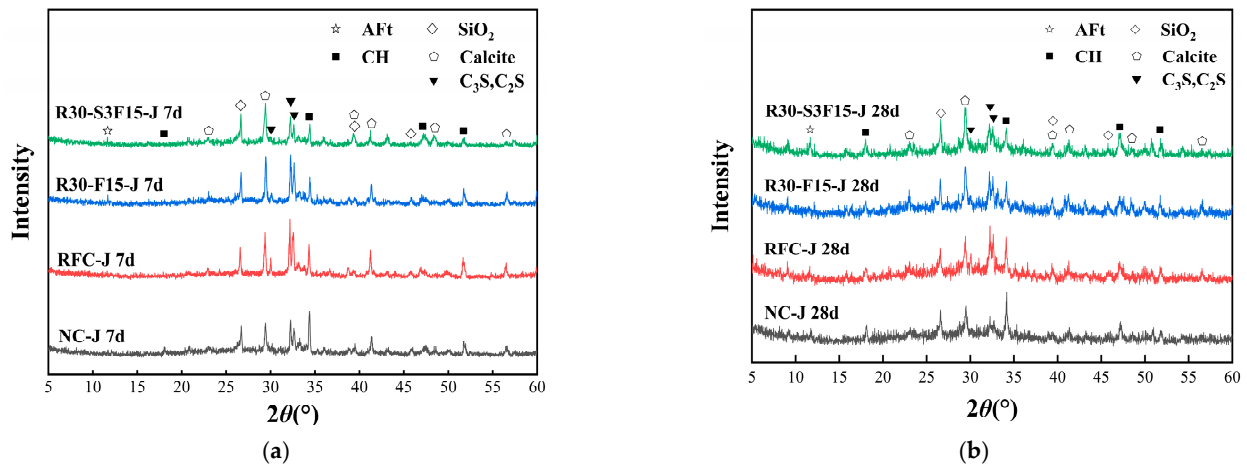


Figure 8. XRD spectra of different cement pastes at different ages. (a) 7 d; (b) 28 d.

The particle size of the CH crystals in the cement paste was calculated by the Scherrer formula, and the equation of the Scherrer formula is as follows:

$$D = K \times \lambda / (B \times \cos\theta) \quad (1)$$

where D is the grain size (nm); K is the Scherrer constant, which generally takes 0.89; λ is the wavelength of the X-ray—the $K_{\alpha 1}$ of Cu target radiation is 0.15405980 (nm); B is the peak half-width of the CH crystals; θ is the diffraction angle of the CH crystals.

As shown in Figure 9, the particle size of the CH crystals corresponding to the 101 crystal faces of RFC-J was larger than that of NC-J. The addition of FA alone and the combination of FA and NS made the particle size of the CH crystals smaller, and NS had a greater influence on the crystal size of CH. Compared with RFC-J, the particle size of the CH crystals in RFC-S3F15-J decreased by 21.7%, which indicated that the addition of FA and NS could refine the grain size of CH and avoid the problem of directional arrangement of CH in ITZ. Zhou et al. reached a similar conclusion [42].

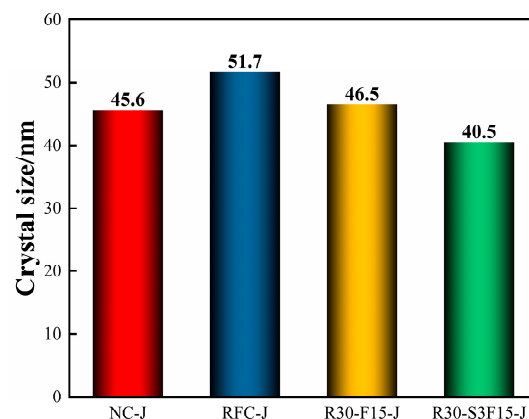


Figure 9. Particle size of CH crystals in different cement pastes.

3.4.2. FTIR

The FTIR spectra of NC-J, RFC-J, RFC-F15-J and RFC-S3F15-J pastes were compared in Figure 10a. It is obvious from the figure that the absorption peak at 875 cm^{-1} was caused by the out-of-plane bending vibration of CO_3^{2-} of CaCO_3 , which may be due to the reaction of CH contained in the paste with CO_2 in the air and the formation of CaCO_3 during the preparation of the cement paste. The absorption peak at 976 cm^{-1} was caused by the Si-O stretching vibration of Q_2 representing $[\text{SiO}_4]^{4-}$, and the absorption peak at 3640 cm^{-1} was caused by the O-H stretching vibration representing CH. Figure 10b is a local enlarged

image at 600–2000 cm^{-1} . The wave number of the Si-O stretching vibration in RFC-F15-J was lower than that in RFC-J, indicating that the hydration degree of RFC-F15-J is poor. A blue-shift phenomenon occurs for RFC-S3F15-J after the addition of FA and NS, and the wave number of the Si-O stretching vibration moves from 972 to 979 cm^{-1} . This indicates that the addition of two materials can increase the degree of polymerization of Q_2 and accelerate the degree of hydration reaction.

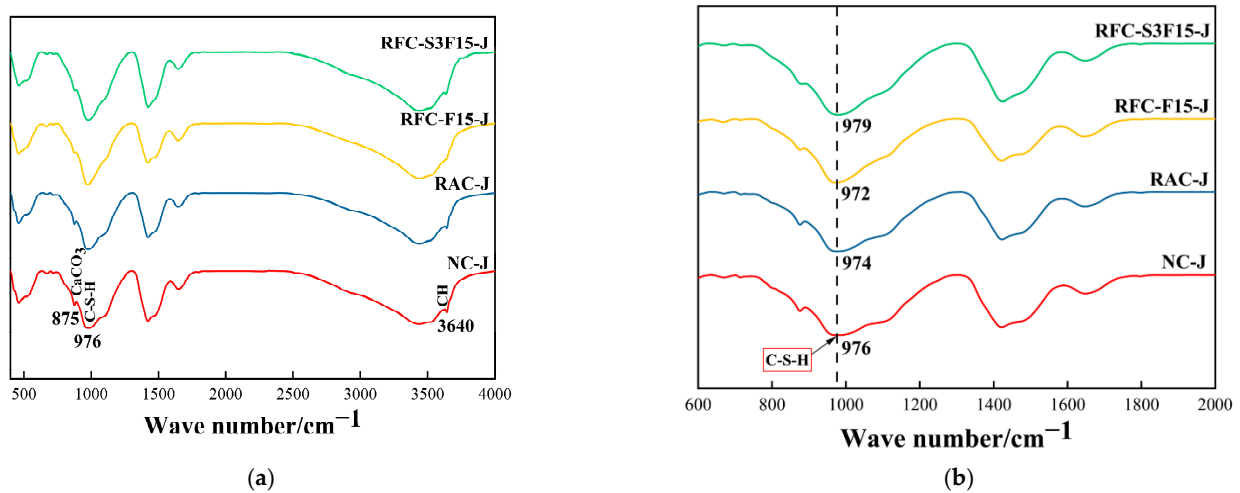


Figure 10. FTIR spectra of different cement pastes. (a) 400–4000 cm^{-1} ; (b) local amplification of 600–2000 cm^{-1} .

3.4.3. SEM

The microstructure of different concrete samples was measured with SEM, as shown in Figure 11. In the RFC samples, there were many large pores and cracks on the surface of the slurry, between the old and new cement pastes and between the slurry and the aggregate (Figure 11a). These pores and cracks may have been caused by uneven vibration during RFC preparation and aggregate detachment during compressive failure. After amplification, it can be seen that large amounts of block CH and needle ettringite (AFt) had grown in the pores, and the connection between the flocculent C-S-H and the crystal was loose, which made the pores poorly filled and prone to become empty again (Figure 11a). These phenomena made the gelation of the slurry in RFC poor, which ultimately degraded its mechanical properties. In contrast, RFC-F15 with fly ash still had obvious pores and cracks, and some of the pores had been filled with slurry (Figure 11c). It was found that the C-S-H in the slurry was wrapped with FA and AFt, and a small amount of bulk CH was embedded in the slurry, thus enhancing the cementitious property of the slurry (Figure 11d). However, RFC-S3F15 with FA and NS exhibited a denser microstructure, and the larger pores were gradually filled into small pores; this effectively alleviated the problem of pore structure damage caused by expansion stress of frozen water due to large pores (Figure 11e). A large amount of flocculent C-S-H wrapped in FA and irregular lumps of CH were found in the enlarged image (Figure 11f), as mentioned above, because the pozzolanic reaction consumes part of CH, and thus the number of CH presented in the image is small. These phenomena indicate that the composite addition of the two materials promoted the hydration reaction, and more C-S-H with strong connection was generated in the hydration products, which were closely combined with other hydration products to improve the cementitious properties of the slurry. Moreover, the secondary hydration reaction reduced the CH content in the hydration products, weakened the phenomenon of ITZ deterioration caused by the directional arrangement of CH, and enhanced the mechanical properties of concrete.

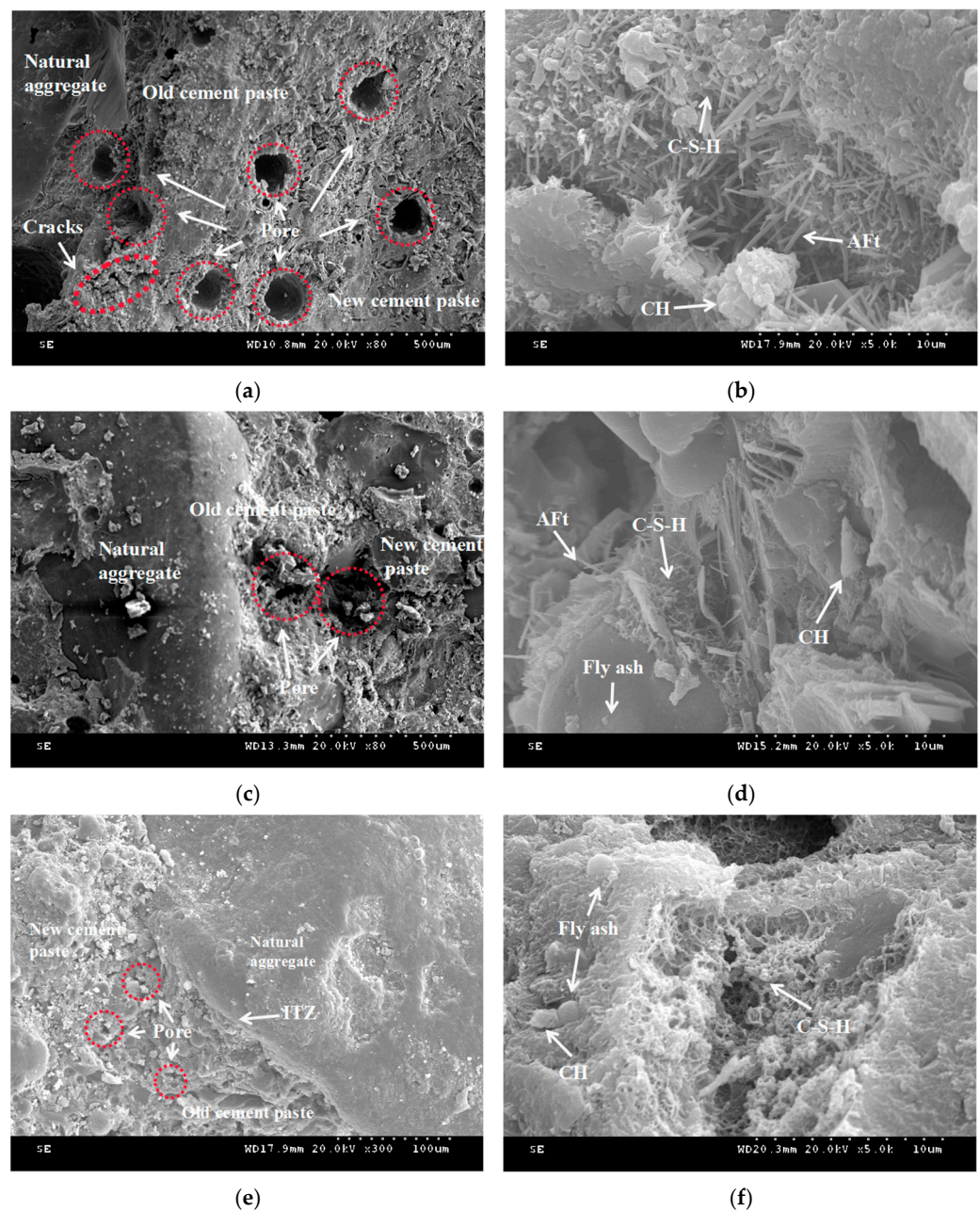


Figure 11. SEM images of different concretes at 28 d. (a) RFC; (b) enlarged RFC; (c) RFC-F15; (d) enlarged RFC-F15; (e) RFC-S3F15; (f) enlarged RFC-S3F15.

3.4.4. EDS

The point scanning analysis of RFC-J, RFC-15 and RFC-S3F15-J cured for 28 days was carried out with EDS, as shown in Figure 12. RFC mainly contains the elements O, Mg, Al, Si, Ca, and Fe. The Ca/Si of RFC-J, RFC-F15-J and RFC-S3F15-J were 2.08, 1.69, 1.17, respectively, and the (Al + Fe)/Ca was 0.2 (Figure 12a,c,e). Taylor et al. found that when $0.8 \leq \text{Ca/Si} \leq 2.5$ and $(\text{Al} + \text{Fe})/\text{Ca} \leq 0.2$, C-S-H was the main hydration product of Portland cement [43]. With the increase of Ca/Si, the content of C-S-H will gradually decrease, while the content of CH and AFt will increase. Compared with RFC-J, the Ca/Si of RFC-F15-J and RFC-S3F15-J decreased by 0.39 and 0.91, indicating that the addition of FA and NS effectively promoted the production of C-S-H.

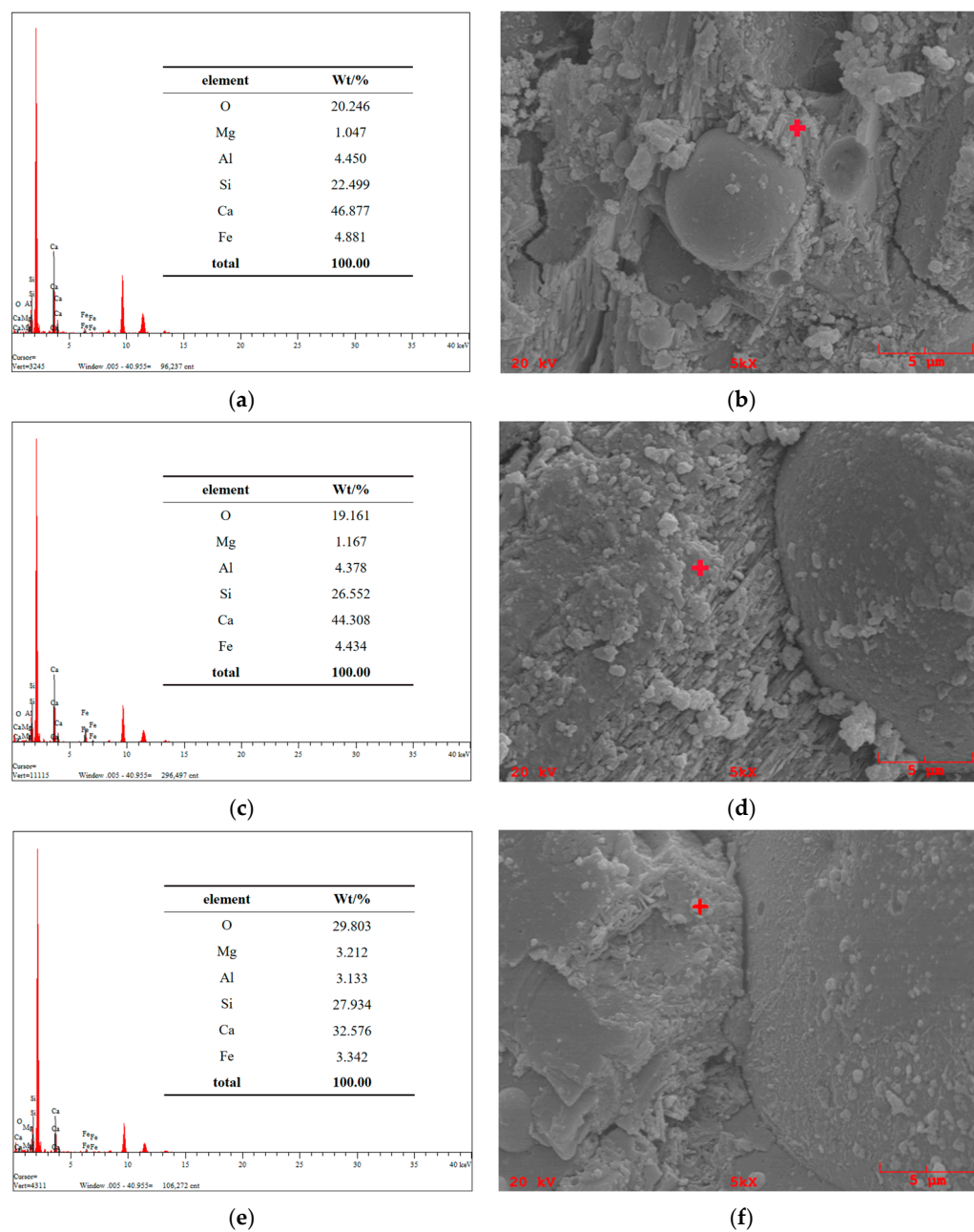


Figure 12. Point scanning images of EDS of different cement pastes at 28d. (a) Element content of RFC-J; (b) point scanning image of RFC-J; (c) element content of RFC-F15-J; (d) point scanning image of RFC-F15-J; (e) element content of RFC-S3F15-J; (f) point scanning image of RFC-S3F15-J.

Figure 13 shows the elemental distribution of RFC and RFC-S3F15 cured for 28 days under EDS mapping scanning. There is a clear boundary between the slurry and the aggregate of RFC (red line area). The Ca element is located below the line, indicating that the area is a cement slurry, and the Si element is enriched above the line, indicating that the area is an aggregate. ITZ is a hollow area between the two elements, and only a small amount of Ca element and Si exist in this area (Figure 13a–c). In contrast, Ca element in RFC-S3F15 is located on both sides of the line, Si element is enriched in the center of the line, and the content of Si element in the Ca element region is significantly increased (Figure 13d–f). In addition, the content of Ca and Si elements in the ITZ region of RFC-S3F15 increased, which may have been caused by more C-S-H filling the ITZ.

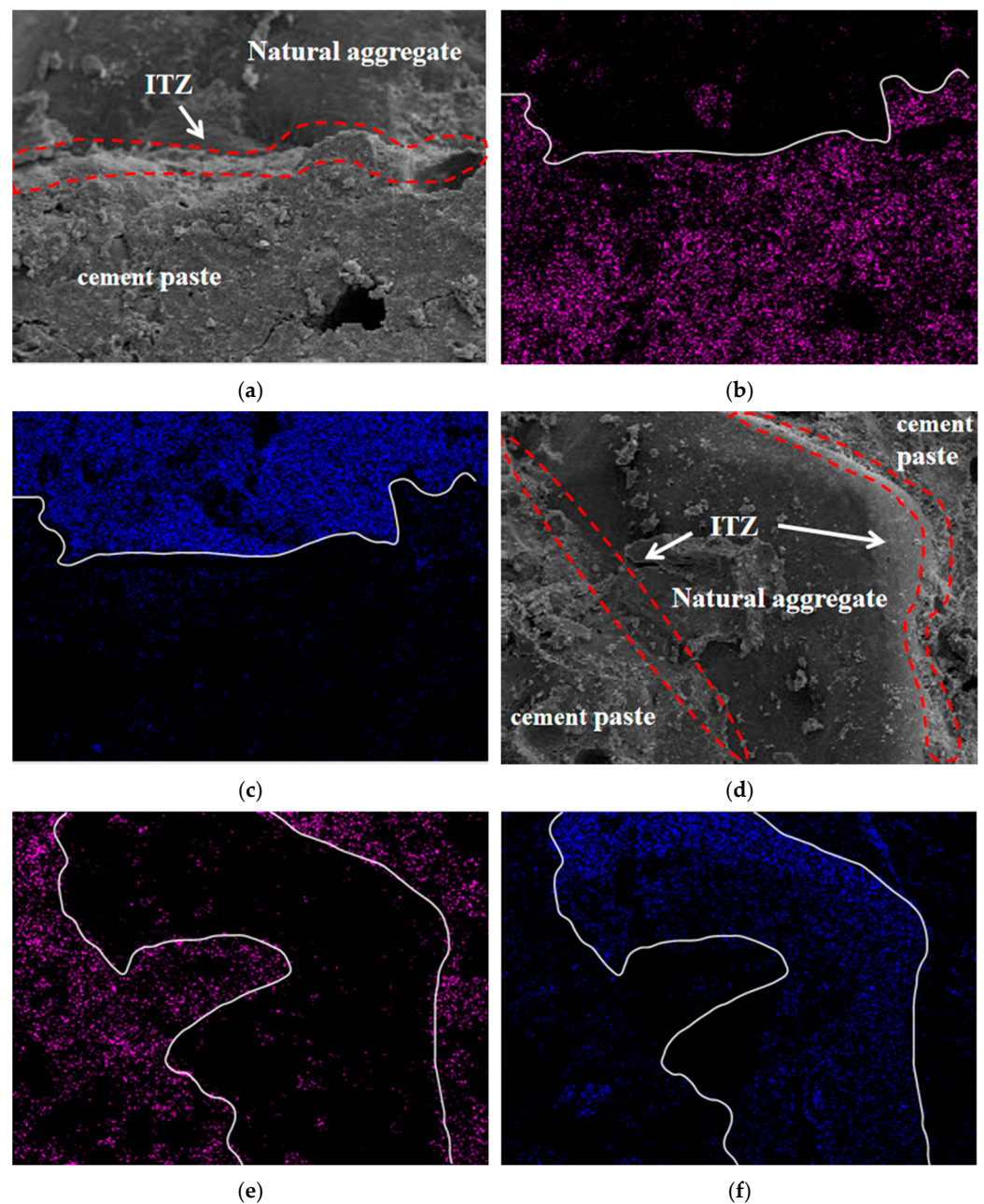


Figure 13. Mapping scanning images of EDS of different concretes at 28 d. (a) Mapping scanning images of RFC; (b) distribution of Ca element in RFC; (c) distribution of Si element in RFC; (d) mapping scanning images of RFC-S3F15; (e) distribution of Ca element in RFC-S3F15; (f) distribution of Si element in RFC-S3F15.

4. Discussion

The results of this study indicated that the SCMs FA and NS have a significant effect on the hydration process and hardening state of RFC directly regenerated from WFC, which is caused by two factors.

4.1. Effect of Nano-Silica on Hydration and Hardening of RFC

Clinker minerals C_3S and C_2S in Portland cement will generate a large number of C-S-H in the hydration reaction, which is the main source of a certain strength of hardened cement stone. As mentioned above, WFC was placed for 180 min in the early hydration reaction, and its cement paste contained a large amount of unreacted C_3S and C_2S clinker minerals. When WFC was again mixed with cement and SCM, C_3S rapidly hydrolyzed in

contact with water, and then Ca^{2+} and OH^- entered the solution and formed a calcium-deficient, silicon-rich layer on its surface. In order to maintain charge balance, the silicon-rich layer absorbed Ca^{2+} to the surface to form an electric double layer as shown in Figure 14. At this time, the dissolved Ca^{2+} and NS made the slurry strongly alkaline. In this alkaline environment, a large amount of $\text{H}_2\text{SiO}_4^{2-}$ in NS was released, which increased the content of $\text{H}_2\text{SiO}_4^{2-}$ in the silicon-rich layer. In order to maintain the charge balance again, the silicon-rich layer continuously absorbed Ca^{2+} in the solution, which made the cement particles continuously dissolve and effectively promote the hydration reaction. In addition, the volcanic ash reaction between NS and CH and its own physical filling gave RFC superior mechanical properties [44].

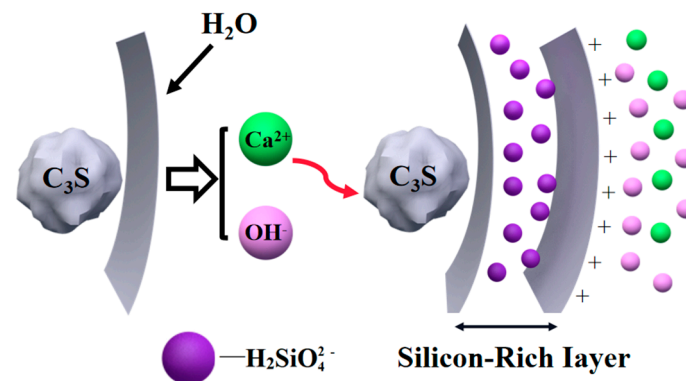


Figure 14. Diagram of silicon-rich layer.

4.2. Effect of Fly Ash on Hydration and Hardening of RFC

During the hydration process, the unevenly dispersed NS can easily cause self-agglomeration and absorb the newly dissolved cement particles in a block or flocculent shape, which hinders the hydration reaction. However, the addition of FA with its small size and smooth surface can effectively reduce the frictional resistance between cement particles and diffuse the cement particles that have been absorbed by NS. In addition, the morphological effect and micro-aggregate effect caused by FA improves the workability and compactness of the paste [45]. FA contains a large number of spherical floating beads and sinking beads, which can play a lubricating role in mixing concrete. In the early stage of hydration, the pozzolanic activity of FA was lower than that of Portland cement, which lead to the decrease of cement composition after replacing cement, delayed the hydration process, and reduced the mechanical properties of concrete. However, in the later stage of slurry hardening, the pozzolanic activity increased, and the floating beads and sinking beads were tightly wrapped by the hydration products C-S-H and AFt, filling in pores and cracks, which can be found in Figure 10f. This phenomenon further improves the mechanical properties of RFC under long-term service conditions.

5. Conclusions

In this paper, unhardened WFC was directly added into fresh concrete to prepare RFC, and FA and NS were added into RFC as SCMs to prepare modified RFC-F and RFC-SF. The effects of FA and NS on the mechanical properties, working performance and freeze–thaw performance of RFC were studied. The microstructure evolution of modified RFC was investigated by XRD, FTIR, SEM and EDS. This study concludes as follows:

- (1) The early strength of RFC-F added with FA alone is poor. The synergistic effect of FA and NS added together makes the early and late mechanical properties of RFC-SF significantly improved. The compressive strength and splitting tensile strength at 7 d are increased by 15.2% and 20.5% at most, and the compressive strength and splitting tensile strength at 90 d are increased by 50.3% and 76.4% at most.

- (2) Adding FA increased the slump of RFC from 150 mm to 185 mm or more; adding NS absorbed free water and reduced the fluidity of concrete. However, the slump of RFC-SF with two materials remains between 120 mm and 185 mm.
- (3) The addition of FA alone improved the freeze–thaw performance of RFC-F, and the combined addition of FA and NS further improved the freeze–thaw performance of RFC-SF. Compared with RFC, the mass loss of RFC-F15 and RFC-S3F15 decreased by 31.9% and 42.6% after freeze–thaw cycles.
- (4) XRD and FTIR showed that the addition of FA delayed the early hydration process of RFC-F. In contrast, the addition of FA and NS accelerated the hydration degree of RFC-SF, reduced the content of CH in the hydration products, and refined the grain size of CH.
- (5) The results of SEM and EDS indicated that the microstructure of RFC-F15 with FA became denser, and the microstructure of RFC-S3F15 with FA and NS was improved obviously, as some pores were filled with C-S-H. Compared with RFC-J, the Ca/Si ratio of RFC-F15-J and RFC-S3F15-J decreased by 0.39 and 0.91.
- (6) As an environmentally friendly material, RFC is conducive to promoting the sustainability of building materials. The effect of more solid wastes such as waste fiber and waste glass on the performance of RFC needs further study, and more efficient recovery methods of WFC need to be actively explored by engineers.

Author Contributions: W.W., D.Z., L.L. and X.Z. are the main contributors of this research work. They carried out the main experimental program, analyzed the experimental results and drafted the research paper; Y.W. mainly processed experimental data and proofread the paper. All authors have read and agreed to the published version of the manuscript.

Funding: This work was financially supported by the Horizontal Project of Qiqihar University. The funder is Qiqihar University, and the funding number is 220122222019.

Data Availability Statement: Data is contained within the article.

Acknowledgments: The authors are grateful for the financial support from Chengbang Ecological Environment Co., Ltd.

Conflicts of Interest: The authors declare no conflict of interest.

References

1. Wang, R.X.; Zhang, Y.X. Recycling fresh concrete waste: A review. *Struct. Concr.* **2018**, *19*, 1939–1955. [[CrossRef](#)]
2. Silva, D.O.F.; Quattrone, M.; Romano, R.C.O.; Angulo, S.C. Reuse of fines from ready-mix concrete washing slurries. *Resour. Conserv. Recycl.* **2020**, *155*, 104653. [[CrossRef](#)]
3. Vieira, L.D.P.; de Figueiredo, A.D.; Moriggi, T.; John, V.M. Waste generation from the production of ready-mixed concrete. *Waste Manag.* **2019**, *94*, 146–152. [[CrossRef](#)] [[PubMed](#)]
4. Nielsen, C.V.; Glavind, M. Danish experiences with a decade of green concrete. *J. Adv. Concert. Technol.* **2007**, *5*, 3–12. [[CrossRef](#)]
5. Zeybek, O.; Ozkilog, Y.O.; Karalar, M.; Celik, A.I.; Qaidi, S.; Ahmad, J.; Burduhos-Nergis, D.D.; Burduhos-Nergis, D.P. Influence of replacing cement with waste glass on mechanical properties of concrete. *Materials* **2022**, *15*, 7513. [[CrossRef](#)] [[PubMed](#)]
6. Karalar, M.; Bilir, T.; Cavuşlu, M.; Özkiliç, Y.O.; Sabri Sabri, M.M. Use of recycled coal bottom ash in reinforced concrete beams as replacement for aggregate. *Front. Mater.* **2022**, *9*, 1064604. [[CrossRef](#)]
7. Qaidi, S.; Najm, H.M.; Abed, S.M.; Ozkilog, Y.O.; Al Dughaihi, H.; Alost, M.; Sabri, M.M.S.; Alkhatib, F.; Milad, A. Concrete containing waste glass as an environmentally friendly aggregate: A review on fresh and mechanical characteristics. *Materials* **2022**, *15*, 6222. [[CrossRef](#)]
8. Celik, A.I.; Ozkilog, Y.O.; Zeybek, O.; Karalar, M.; Qaidi, S.; Ahmad, J.; Burduhos-Nergis, D.D.; Bejinariu, C. Mechanical behavior of crushed waste glass as replacement of aggregates. *Materials* **2022**, *15*, 8093. [[CrossRef](#)]
9. Basaran, B.; Kalkan, I.; Aksoylu, C.; Özkiliç, Y.O.; Sabri, M.M.S. Effects of Waste Powder, Fine and Coarse Marble Aggregates on Concrete Compressive Strength. *Sustainability* **2022**, *14*, 14388. [[CrossRef](#)]
10. Audo, M.; Mahieux, P.Y.; Turcry, P. Utilization of sludge from ready-mixed concrete plants as a substitute for limestone fillers. *Constr. Build. Mater.* **2016**, *112*, 790–799. [[CrossRef](#)]
11. Xuan, D.X.; Poon, C.S.; Zheng, W. Management and sustainable utilization of processing wastes from ready-mixed concrete plants in construction: A review. *Resour. Conserv. Recycl.* **2018**, *136*, 238–247. [[CrossRef](#)]
12. He, X.Y.; Ma, Q.H.; Su, Y.; Zheng, Z.Q.; Tan, H.B.; Peng, K.; Zhao, R.X. Humid hardened concrete waste treated by multiple wet-grinding and its reuse in concrete. *Constr. Build. Mater.* **2022**, *350*, 128485. [[CrossRef](#)]

13. Vieira, L.D.P.; de Figueiredo, A.D. Evaluation of concrete recycling system efficiency for ready-mix concrete plants. *Waste Manag.* **2016**, *56*, 337–351. [[CrossRef](#)]
14. Wang, X.; Yan, Y.R.; Tong, X.F.; Gong, Y.F. Investigation of mineral admixtures on mechanical properties of alkali-activated recycled concrete powders cement. *Buildings* **2022**, *12*, 1234. [[CrossRef](#)]
15. Asadollahfardi, G.; Asadi, M.; Jafari, H.; Moradi, A.; Asadollahfardi, R. Experimental and statistical studies of using wash water from ready-mix concrete trucks and a batching plant in the production of fresh concrete. *Constr. Build. Mater.* **2015**, *98*, 305–314. [[CrossRef](#)]
16. Reiterman, P.; Mondschein, P.; Doušová, B.; Davidová, V.; Keppert, M. Utilization of concrete slurry waste for soil stabilization. *Case Stud. Constr. Mater.* **2022**, *16*, e00900. [[CrossRef](#)]
17. Zhang, J.; Fujiwara, T. Concrete sludge powder for soil stabilization. *Transp. Res. Rec. J. Transp. Res. Board* **2007**, *2026*, 54–59. [[CrossRef](#)]
18. Iizuka, A.; Sakai, Y.; Yamasaki, A.; Honma, M.; Hayakawa, Y.; Yanagisawa, Y. Bench-scale operation of a concrete sludge recycling plant. *Ind. Eng. Chem. Res.* **2012**, *51*, 6099–6104. [[CrossRef](#)]
19. Iizuka, A.; Sasaki, T.; Hongo, T.; Honma, M.; Hayakawa, Y.; Yamasaki, A.; Yanagisawa, Y. Phosphorus adsorbent derived from concrete sludge (PAdeCS) and its phosphorus recovery performance. *Ind. Eng. Chem. Res.* **2012**, *51*, 11266–11273. [[CrossRef](#)]
20. Sasaki, T.; Sakai, Y.; Iizuka, A.; Nakae, T.; Kato, S.; Kojima, T.; Yamasaki, A. Evaluation of the capacity of hydroxyapatite prepared from concrete sludge to remove lead from water. *Ind. Eng. Chem. Res.* **2011**, *50*, 9564–9568. [[CrossRef](#)]
21. Xuan, D.X.; Zhan, B.J.; Poon, C.S.; Zheng, W. Innovative reuse of concrete slurry waste from ready-mixed concrete plants in construction products. *J. Hazard. Mater.* **2016**, *312*, 65–72. [[CrossRef](#)] [[PubMed](#)]
22. Lobo, C.; Guthrie, W.F.; Kacker, R. A Study on the reuse of plastic concrete using extended set-retarding admixtures. *J. Res. Natl. Inst. Stand. Technol.* **1995**, *100*, 575–589. [[CrossRef](#)] [[PubMed](#)]
23. Okawa, Y.; Yamamiya, H.; Nishibayashi, S. Study on the reuse of returned concrete. *Mag. Concr. Res.* **2000**, *52*, 109–115. [[CrossRef](#)]
24. Vieira, L.D.P.; Figueiredo, A.D. Implementation of the use of hydration stabilizer admixtures at a ready-mix concrete plant. *Case Stud. Constr. Mater.* **2020**, *12*, e00334. [[CrossRef](#)]
25. Kong, D.Y.; He, G.P.; Pan, H.W.; Weng, Y.H.; Du, N.; Sheng, J.S. Influences and mechanisms of nano-C-S-H gel addition on fresh properties of the cement-based materials with sucrose as retarder. *Materials* **2020**, *13*, 2345. [[CrossRef](#)]
26. Lothenbach, B.; Scrivener, K.; Hooton, R.D. Supplementary cementitious materials. *Cem. Concr. Res.* **2011**, *41*, 1244–1256. [[CrossRef](#)]
27. Wang, B.; Xiao, H.; Zhang, T. Autogenous shrinkage property of high-performance multi-walled cement-based carbon nanotubes composites. *J. Nanosci. Nanotechnol.* **2018**, *18*, 6894–6904. [[CrossRef](#)]
28. Gholampour, A.; Kiamahalleh, M.V.; Tran, D.N.H.; Ozbakkaloglu, T.; Losic, D. Revealing the dependence of the physiochemical and mechanical properties of cement composites on graphene oxide concentration. *RSC Adv.* **2017**, *7*, 55148–55156. [[CrossRef](#)]
29. Hasan-Nattaj, F.; Nematzadeh, M. The effect of forta-ferro and steel fibers on mechanical properties of high-strength concrete with and without silica fume and nano-silica. *Constr. Build. Mater.* **2017**, *137*, 557–572. [[CrossRef](#)]
30. Wang, J.B.; Du, P.; Zhou, Z.H.; Xu, D.Y.; Xie, N.; Cheng, X. Effect of nano-silica on hydration, microstructure of alkali-activated slag. *Constr. Build. Mater.* **2019**, *220*, 110–118. [[CrossRef](#)]
31. Shan, H.L.; Yu, Z.P. Strength, chloride ion penetration, and nanoscale characteristics of concrete prepared with nano-silica slurry pre-coated recycled aggregate. *Buildings* **2022**, *12*, 1707. [[CrossRef](#)]
32. Kong, D.Y.; Su, Y.; Du, X.F.; Yang, Y.; Wei, S.; Shah, S.P. Influence of nano-silica agglomeration on fresh properties of cement pastes. *Constr. Build. Mater.* **2013**, *43*, 557–562. [[CrossRef](#)]
33. Elahi, A.; Basheer, P.A.M.; Nanukuttan, S.V.; Khan, Q.U.Z. Mechanical and durability properties of high performance concretes containing supplementary cementitious materials. *Constr. Build. Mater.* **2010**, *24*, 292–299. [[CrossRef](#)]
34. Kim, K.; Shin, M.; Cha, S. Combined effects of recycled aggregate and fly ash towards concrete sustainability. *Constr. Build. Mater.* **2013**, *48*, 499–507. [[CrossRef](#)]
35. Yoshitake, I.; Zhang, W.B.; Mimura, Y.; Saito, T. Uniaxial tensile strength and tensile Young's modulus of fly-ash concrete at early age. *Constr. Build. Mater.* **2013**, *40*, 514–521. [[CrossRef](#)]
36. Cui, K.; Chang, J. Hydration, reinforcing mechanism, and macro performance of multi-layer graphene-modified cement composites. *J. Build. Eng.* **2022**, *57*, 104880. [[CrossRef](#)]
37. Gebremichael, N.N.; Karein, S.M.M.; Karakouzian, M.; Jadidi, K. Investigation of setting time and compressive strength of ready-mixed concrete blended with returned fresh concrete. *Constr. Build. Mater.* **2019**, *197*, 428–435. [[CrossRef](#)]
38. Feng, P.; Chang, H.L.; Liu, X.; Ye, S.X.; Shu, X.; Ran, Q.P. The significance of dispersion of nano-SiO₂ on early age hydration of cement pastes. *Mater. Des.* **2020**, *186*, 108320. [[CrossRef](#)]
39. Reches, Y.; Thomson, K.; Helbing, M.; Kosson, D.S.; Sanchez, F. Agglomeration and reactivity of nanoparticles of SiO₂, TiO₂, Al₂O₃, Fe₂O₃, and clays in cement pastes and effects on compressive strength at ambient and elevated temperatures. *Constr. Build. Mater.* **2018**, *167*, 860–873. [[CrossRef](#)]
40. Wang, J.B.; Liu, M.L.; Wang, Y.G.; Zhou, Z.H.; Xu, D.Y.; Du, P.; Cheng, X. Synergistic effects of nano-silica and fly ash on properties of cement-based composites. *Constr. Build. Mater.* **2020**, *262*, 120737. [[CrossRef](#)]
41. Sun, H.L.; Zhang, X.Z.; Zhao, P.; Liu, D. Effects of nano-Silica particle size on fresh state properties of cement paste. *KSCE J. Civ. Eng.* **2021**, *25*, 2555–2566. [[CrossRef](#)]

42. Zhou, S.; Zhang, X.T.; Zhou, H.; Li, D.X. Effects of graphene oxide encapsulated silica fume and its mixing with nano-silica sol on properties of fly ash-mixed cement composites. *Crystals* **2022**, *12*, 144. [[CrossRef](#)]
43. Taylor, H.F.W.; Newbury, D.E. An electron-microprobe study of a mature cement paste. *Cem. Concr. Res.* **1984**, *14*, 565–573. [[CrossRef](#)]
44. Singh, L.P.; Karade, S.R.; Bhattacharyya, S.K.; Yousuf, M.M.; Ahalawat, S. Beneficial role of nanosilica in cement based materials—A review. *Constr. Build. Mater.* **2013**, *47*, 1069–1077. [[CrossRef](#)]
45. Bilir, T.; Gencil, O.; Topcu, I.B. Properties of mortars with fly ash as fine aggregate. *Constr. Build. Mater.* **2015**, *93*, 782–789. [[CrossRef](#)]

Disclaimer/Publisher’s Note: The statements, opinions and data contained in all publications are solely those of the individual author(s) and contributor(s) and not of MDPI and/or the editor(s). MDPI and/or the editor(s) disclaim responsibility for any injury to people or property resulting from any ideas, methods, instructions or products referred to in the content.